Spectrochimica Acta Part A: Molecular and Biomolecular Spectroscopy 246 (2021) 118944

Contents lists available at ScienceDirect

Spectrochimica Acta Part A: Molecular and Biomolecular Spectroscopy

journal homepage: www.elsevier.com/locate/saa

Discovery of novel dehydroabietic acid derivatives as DNA/BSA binding and anticancer agents

Lin-Ying Li [a,b,1], Bao-Li Fei [a,b,c,*,1], Pingping Wang [a], Ling-Yan Kong [d], Jian-Ying Long [e]

[a] Jiangsu Key Lab of Biomass-based Green Fuels and Chemicals, College of Chemical Engineering, Nanjing Forestry University, Nanjing 210037, China
[b] Jiangsu Co-Innovation Center of Efficient Processing and Utilization of Forest Resources, Nanjing Forestry University, Nanjing 210037, China
[c] State Key Laboratory for Chemistry and Molecular Engineering of Medicinal Resources, Guangxi Normal University, Guilin 541004, China
[d] College of Food Science and Engineering, Nanjing University of Finance and Economics, Nanjing 210023, China
[e] College of Science, Nanjing Forestry University, Nanjing 210037, China

ARTICLE INFO

Article history:
Received 12 July 2020
Received in revised form 27 August 2020
Accepted 3 September 2020
Available online 15 September 2020

Keywords:
Rosin derivative
Amide
DNA
BSA
Anticancer

ABSTRACT

To explore the biological properties of rosin derivatives, two dehydroabietic acid derivatives N-(5-dehydroabietyl-1,3,4-thiadiazole)-yl-pyridine-2-carboxamide (DTPC) and di-N-(5-dehydroabietyl-1,3,4-thiadiazole)-yl-pyridine-2,6-carboxamide (DDTPC) with 1,3,4-thiadiazole, pyridine and amide moieties were designed and synthesized according to superposition principle of activity group. They interact with calf thymus DNA (CT DNA) via intercalation based on the results of circular dichroism (CD) and fluorescence spectroscopy, DNA denaturation and viscosity studies. Fluorescence and CD spectral experiments indicate that they might be transported and stored by protein like bovine serum albumin (BSA). MTT assay was further carried out to examine their cytotoxicity, they both showed selective cytotoxicity and DTPC exhibited better cytotoxicity. The antiproliferative effect of DTPC toward A431 cell line was stronger than that of clinically used cisplatin and oxaliplatin. In addition, the cytotoxicity of DTPC and DDTPC was closely related with their DNA binding ability.

1. Introduction

Cancer is a serious threat to human health and life, but there is no way or drug to cure cancer completely at the moment. Even though chemotherapy is an important means to treat cancer, it still has some defects such as poor selectivity, drug resistance and side effects [1]. Therefore, scientists in related fields are trying to find more effective anticancer drugs. Natural products (NPs) and their derivatives play an important role in the research of anticancer drugs, nearly 60% of clinically approved anticancer drugs are associated with NPs [1].

Rosin is the secretion of pine trees, as a kind of natural resin, its rich resources together with its favorable biocompatibility and biodegradability, make rosin and its derivatives attract a lots of attention in many fields such as cosmetics, food additives, agrochemicals and pharmaceutical applications [2,3]. Rosin derivatives have a wide range of biological activities, such as antiulcer, antimicrobial, anxiolytic, antiviral, antitumor and cytotoxic activities [4]. Dehydroabietic acid (DHA) with diterpene structure and three chiral carbon atoms, is one of the main modified products of traditional Chinese medicine rosin. DHA itself and its organic derivatives have anti-inflammatory, anti-bacterial and antitumor activities [5]. In addition, DHA is cheap and easy to be gained in optically pure form and carried out structural modification according to requirement. To modify DHA and broad its application fields has always been a frontier research field of forest chemistry and industry. 1,3,4-thiadiazole is an attractive heterocyclic compound in medicinal and pharmaceutical chemistry [4], and 2-amino-1,3,4-thiadiazole had entered the phase II clinical trial as a tumor inhibitor [4]. Pyridine ring is often used as a building block in natural products and synthetic drugs, its derivatives have been widely used in pharmaceutical chemistry with broad spectrum of biological activities [6].

DNA and protein are basic macromolecules and important targets for some drugs in vivo. To understand the interaction mechanism between candidate drugs and such biomacromolecules, is of great significance to elucidate the structure-activity relationship and pharmacodynamic mechanism of drugs. Therefore, to study the interaction mechanism of compounds with DNA and protein is the basis of developing new drugs [7,8].

We have been working to develop the biological properties of rosin derivatives, in consideration of the attractive medicinal and pharmaceutical values of amide, pyridine and 1,3,4-thiadiazole moieties [9–12], two optically pure chiral DHA derivatives (**8** and **9**) containing the above mentioned units were synthesized (Scheme 1), and their DNA/

* Corresponding author at: Jiangsu Key Lab of Biomass-based Green Fuels and Chemicals, College of Chemical Engineering, Nanjing Forestry University, Nanjing 210037, China.
E-mail address: hgfbl@njfu.edu.cn (B.-L. Fei).
[1] These authors contributed equally to this work.

https://doi.org/10.1016/j.saa.2020.118944
1386-1425/

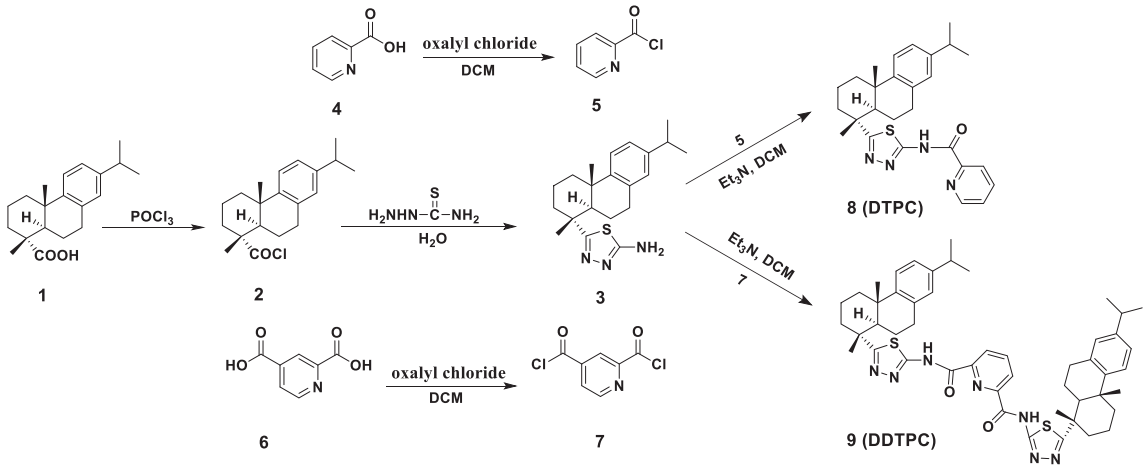

Scheme 1. Synthesis route of the target compounds **8** and **9**.

BSA binding abilities and primary cytotoxic activities were studied here. We tried to explore the relationship between the cytotoxic activities and DNA/BSA binding affinities of such compounds.

2. Materials and methods

2.1. Materials and instruments

All the chemicals and solvents were obtained from commercial sources and used as received, except DHA and dichloromethane (DCM) were purified according to the standard procedures.

$^{1}H/^{13}C$ NMR, IR, circular dichroism (CD), UV–vis, fluorescence, viscosity and C, H and N analysis were carried out on Bruker Avance III HD 600 MHz spectrometer (Switzerland), Nicolet 380 FT-IR spectrometer, Jasco J-810 spectropolarimeter, TU-1901 UV–vis spectrophotometer (Beijing Purkinje General Instrument Co., Ltd), Perkin-Elmer LS-55 fluorescence spectrophotometer, Ubbelodhe viscometer and Elementar Vario Micro elemental analyzer, respectively.

2.2. Synthesis

The synthetic procedure is shown in Scheme 1. **2**, **3** and N-(5-dehydroabietyl-1,3,4-thiadiazole)-yl-pyridine-2-carboxamide (**8**) were prepared according to literature [1]. The synthesis of **5** and **7** were based on the literature method [13,14].

2.2.1. Synthesis of N-(5-dehydroabietyl-1,3,4-thiadiazole)-yl-pyridine-2-carboxamide (*8*)

Triethylamine (2 mL) and **2** (1.42 g, 10 mmol) were dissolved in 20 mL dry dichloromethane, respectively, and then added dropwise to the solution of **3** (3.55 g, 10 mmol) in 30 mL dry dichloromethane, separately, under the condition of ice bath and vigorously stirring. The reaction process was monitored by thin layer chromatography (TLC), 4 h later, 30 mL water was added to the above mixture and quenched the reaction. Then, the organic phase was separated and the aqueous phase was extracted with dichloromethane (3 × 20 mL). The combined organic phase was dried with $MgSO_4$ overnight. After filtration and reduced evaporation, the obtained crude product was purified by column chromatography on silica, eluted with petroleum ether-ethyl acetate (3:1) to give **8** as white powders in 63% yield. Single crystal suitable for X-ray diffraction was obtained by slow evaporation the solution of **8** in methanol and water (v/v = 9:1). m.p. 135–137 °C. CD (nm): 195 (positive), 200 (negative), 205 (positive), 213 (negative), 221 (negative), 230 (positive). Anal. cald. for $C_{27}H_{32}N_4OS$ (%): C, 70.40; H, 7.00; N, 12.16; found: C, 70.42; H, 6.98; N, 12.15. MS (*m/z*): 461.2 $[M+1]^+$. IR (ν, cm^{-1}, KBr pellet): 3346, 3259, 3247, 2854, 2763, 1604, 1432, 1311. ^{1}H NMR (600 MHz, $CDCl_3$), δ (ppm): 8.704 (1H, d, J = 4.8 Hz), 8.277(1H, d, J = 7.8 Hz), 7.935–7.964 (1H, m), 7.561–7.583 (1H, m), 7.203 (1H, d, J = 7.8 Hz), 7.011–7.027 (1H, m), 6.864 (1H, d, J = 1.2 Hz), 2.805–2.855 (3H, m), 2.415 (1H, d, J = 12.6 Hz), 2.168 (1H, dd, J = 12.6, 1.8 Hz), 1.816–1.967 (6H, m), 1.655 (3H, s), 1.548–1.622 (1H, m), 1.473–1.506 (1H, m), 1.329 (3H, s), 1.224 (6H, d, J = 6.6 Hz). ^{13}C NMR (101 MHz, $CDCl_3$), δ (ppm): 177.69, 161.90, 158.06, 148.80, 147.42, 146.67, 145.91, 137.90, 134.69, 127.71, 127.01, 124.18, 124.06, 123.17, 77.48, 77.16, 76.84, 50.89, 44.31, 42.73, 38.29, 38.00, 33.56, 30.13, 25.71, 24.11, 24.05, 20.61, 19.33, 19.24.

2.2.2. Synthesis of di-N-(5-dehydroabietyl-1,3,4-thiadiazole)-yl-pyridine-2,6-carboxamide (*9*)

Triethylamine (4 mL) and **2** (2.04 g, 20 mmol) were dissolved in 40 mL dry dichloromethane, respectively, and then added dropwise to the solution of **3** (3.55 g, 10 mmol) in 60 mL dry DCM, separately, under the condition of ice bath and vigorously stirring. The reaction progress was monitored by TLC. 24 h later, the reaction solution was washed alternately with 5% HCl (3 × 45 mL) and saturated $NaHCO_3$ (3 × 45 mL). The resulted organic phase was collected, combined with the DCM extraction of the aqueous phase, and dried with $MgSO_4$ overnight. The crude product was obtained after getting rid of DCM, white powder could be afforded after recrystallization from the mixed solvent of methanol and DCM (v/v = 3:1) in 63% yield. Single crystal suitable for X-ray diffraction was obtained by diffusion of acetone into tetrahydrofuran solution of **9**. m.p. 244–245 °C. CD (nm): 195 (positive), 200 (negative), 205 (positive), 213 (negative), 221 (negative), 230 (positive). Anal. cald. for $C_{49}H_{59}N_7O_2S_2$ (%): C, 69.88; H, 7.06; N, 11.64; found: C, 69.90; H, 7.04; N, 11.65. MS (*m/z*): 842.18 $[M]^+$. IR (ν, cm^{-1}, KBr pellet): 3320, 3145, 2859, 2827, 2777, 1585, 1438, 1363. ^{1}H NMR (600 MHz, CDCl3), δ (ppm): 8.480 (2H, d, J = 7.8 Hz), 8.123–8.149 (1H, m), 7.187 (2H, d, J = 8.4 Hz), 7.006–7.023 (2H, m), 6.842 (2H, d, J = 1.2 Hz), 3.751–3.773 (2H, m), 2.694–2.848 (6H, m), 2.385 (2H, d, J = 13.2 Hz), 2.097 (2H, dd, J = 12, 1.8 Hz), 1.747–1.872 (12H, m), 1.553 (6H, s), 1.384–1.419 (2H, m), 1.292 (6H, s), 1.225 (12H, d, J = 7.2 Hz). ^{13}C NMR (101 MHz, $CDCl_3$), δ (ppm): 177.38, 161.37, 158.90, 147.26, 146.54, 145.82, 139.53, 134.52, 126.92, 126.74, 124.07, 123.97, 68.00, 50.49, 44.10, 42.54, 38.12, 37.82, 33.48, 30.98, 29.97, 25.65, 25.55, 24.03, 23.98, 20.50, 19.17, 19.12.

2.3. DNA and BSA binding studies

The corresponding techniques are referred to the methods used in the published papers of our group [1].

2.4. MTT assay

The procedure for MTT assay was described by us before [1]. The selected cells were treated with cisplatin, oxaliplatin, **3**, **8** and **9** of dissimilar concentrations (0.1, 1, 2, 5, 10, 20 μM) for a period of 48 h.

2.5. X-ray crystallography

Diffraction intensities for **8** and **9** were collected at 293(2) K (**8**) and 273(2) K (**9**) on Bruker D8 Venture (**8**) and Bruker Apex II CCD (**9**) diffractometers with graphite-monochromated Mo-K*a* radiation (λ = 0.71073 Å). Absorption corrections were applied using SADABS. SHELXTL-97 program package was used to solve the structures of **8** and **9** directly. All H atoms were positioned geometrically and treated as riding on their parent atoms. CCDC reference number: 2012691 (**8**) and 2012691 (**9**).

3. Results and discussion

3.1. Description of the crystal structures

The compounds **8** and **9** crystallized in orthorhombic system with chiral space group $P2_12_12_1$. The crystal data and refinement for them are given in Table 1, and the important bond lengths and angles are listed in Table S1. The crystal structures of them are shown in Fig. 1. The molecule number in the unit cell of **8** and **9** is two and one, respectively. The two cyclohexane rings of the dehydroabietyl group adopt classic chair and half-chair conformations, respectively [15]. The benzene ring and the pyridine ring are basically planar. The two methyl groups are in the axis position of the cyclohexane ring belonging to the dehydroabietyl group [15].

3.2. DNA binding study

The ethidium bromide (EB) displacement assay is a sensitive and widely accepted method to study the interaction mode between small molecules and DNA. When EB molecules insert into the base pairs of DNA, the DNA-EB system will emit the characteristic fluorescence of EB [16]. If the other small molecules insert into DNA base pairs occupied with EB, EB will be squeezed out and thus the EB fluorescence intensity of the DNA-EB system will be weakened [16]. As indicated in Fig. 2, the fluorescence intensity of CT DNA-EB system at 600 nm decreased evidently with the addition of increasing amount of **8** and **9**. This phenomenon indicates that **8** and **9** competed with EB for the binding positions of DNA and displaced EB, resulting in fluorescence quenching of the DNA-EB system. The following Stern-Volmer equation was employed to estimate the quenching effect of **8** and **9** [15].

$$F_0/F = 1 + K_{SV}[Q] \quad (1)$$

where F_0 and F are the fluorescence intensities of EB-DNA system in the absence and present of quencher (**8**/**9**), respectively. K_{SV} is the Stern-Volmer quenching constant, and [Q] is the concentration of the quencher [15]. The K_{SV} values of **8** and **9** are 3.74×10^4 L mol^{-1} and 2.54×10^4 L mol^{-1}, respectively (insets in Fig. 2). Such data suggest that they could bind with CT DNA and **8** had stronger binding affinity.

The DNA thermal denaturation experiment is a favorable method to investigate the interaction between small molecules and DNA. At the DNA melting temperature (T_m), half of DNA exists in the single-stranded state and the other half exists in double-stranded state and there is an equilibrium between the two forms [17]. When a small molecule interacts with DNA, the change of T_m (ΔT_m) can be observed according to the interaction mode. In general, intercalation can cause an alteration of 5 °C to 8 °C, while groove or electrostatic binding generates small or no change [1]. Fig. 3 displays that the addition of **8** and **9** increased the T_m of CT DNA from 78.10 °C to, and 83.86 °C (**8**) and 81.90 °C (**9**), the corresponding ΔT_m were 5.76 °C (**8**) and 3.80 °C (**9**), respectively. These data illustrate that **8** was a more effective binder.

CD spectroscopy was often used to evaluate the disturbance of DNA secondary structure caused by its interaction with small molecule. In the CD spectra of CT DNA, there are two characteristic bands around 278 nm (positive) and 248 nm (negative), which are derived from the base stacking and the right-handed helicity of B-type CT DNA [1]. For the positive band, both **8** and **9** increased its intensity; for the negative band, **8** reduced its intensity while **9** increased its intensity, and **8** produced more evident changes in terms of the magnitude (Fig. 4). This result indicates that their influence patterns on DNA structure were not the same, and **8** had stronger DNA binding ability. The absence of red or blue shift of the characteristic bands demonstrates that there was no significant change in the B-type CT DNA conformation.

Viscosity experiment as a hydrodynamic technique is accurate to study the interaction mode between DNA and small molecules [1].

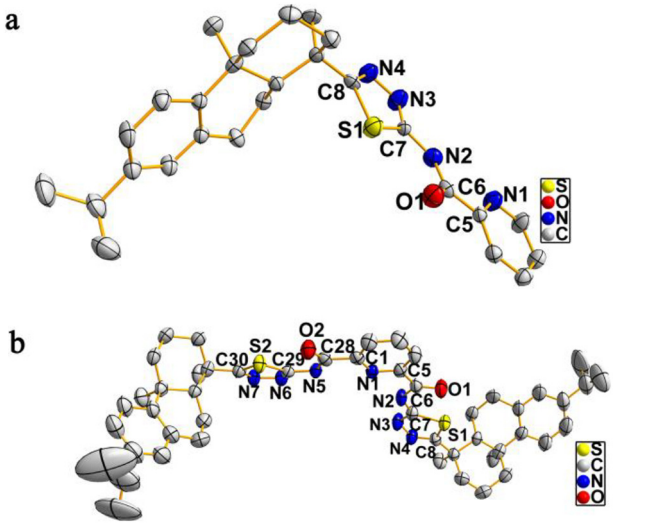

Fig. 1. ORTEP views of molecular structures of **8** (a) and **9** (b) with the ellipsoids drawn at the 40% probability, hydrogen atoms and solvent molecule are omitted for clarity.

Table 1
Crystallographic data and structure refinement parameters for **8** and **9**.

Compounds	**8**	**9**
Empirical formula	$C_{54}H_{64}N_8O_2S_2$	$C_{53}H_{67}N_7O_3S_2$
Formula weight	921.25	914.26
T/K	293	273
Wavelength/Å	0.71073	0.71073
Crystal system	Orthorhombic	Orthorhombic
Space group	$P2_12_12_1$	$P2_12_12_1$
a/Å	8.280(2)	18.5951(7)
b/Å	57.679(16)	24.8535(9)
c/Å	10.527(3)	10.9078(4)
V/Å^3	5028(2)	5041.1(3)
Z	4	4
D_c/(g·cm^{-3})	1.217	1.205
μ(Mo Kα)/mm^{-1}	0.16	0.16
F(000)	1968	1960
Crystal size/mm^3	0.31 × 0.25 × 0.22	0.20 × 0.18 × 0.15
Data measured	20,554	34,549
R(int)	0.100	0.049
Unique data	8542	8880
Unique data with $I > 2$ (I)	4311	5361
Parameters/restraints	595/18	594/1
wR_2 (all data)	0.142	0.118
S (all data)	1.02	1.00
R_1 [$I > 2\sigma(I)$]	0.081	0.053
GOF on F^2	1.025	1.002
Flack parameter	−0.01(10)	0.04(7)
Largest diff. peak and hole/(e Å^{-3})	0.22/−0.26	0.27/−0.13

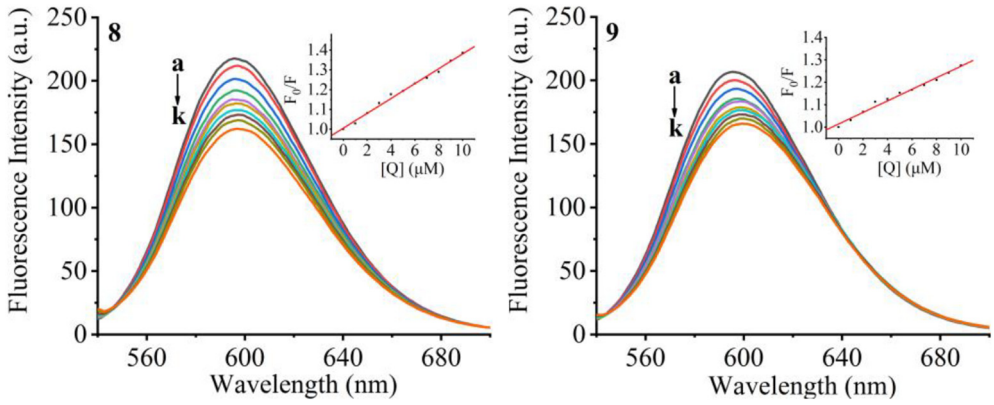

Fig. 2. Effects of **8** and **9** on the emission spectra of EB-CT DNA system at 298 K and pH 7.2, [DNA] = 1.0×10^{-4} M, [**4**/**5**/**6**]/[DNA] = 0, 0.01, 0.02, 0.03, 0.04, 0.05, 0.06, 0.07, 0.08, 0.09, 0.1. Insets: plot of F_0/F versus [Quencher].

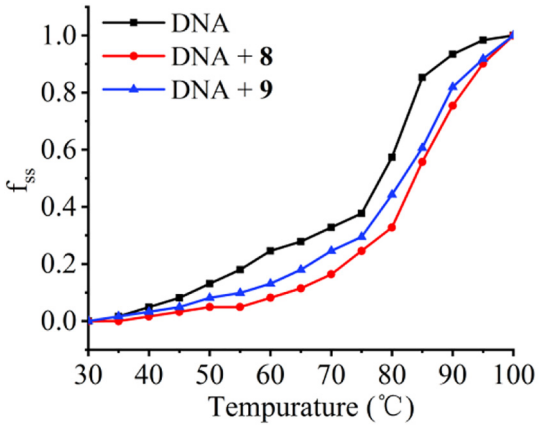

Fig. 3. Melting curves of CT DNA in the absence and presence of **8**/**9** at 298 K and pH 7.2, [DNA] = 5.0×10^{-5} M, [**8**/**9**]/[DNA] = 0.2.

Viscosity analysis is sensitive to reflect the DNA length change. As a general rule, classical intercalation can increase the length of DNA and promote an increase in viscosity, while groove or electrostatic binding can bend or kink the DNA helix, which cause reduction or no change in DNA length and viscosity [1]. It is seen in Fig. 5 that with the addition of increased amounts of EB, **8** and **9** into the CT DNA solution, the viscosity of DNA gradually increased and the effect of **8** was more significant.

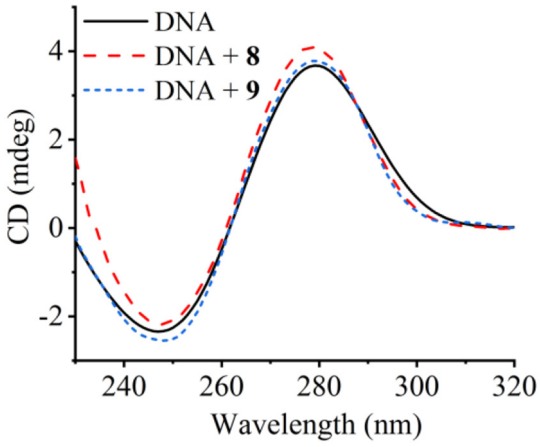

Fig. 4. Effects of **8** and **9** on the CD spectra of DNA at 298 K and pH 7.2, [DNA] = 5.0×10^{-5} M, [**8**/**9**]/[DNA] = 0.2.

So far, it can be considered that the binding mode between CT DNA and **8**/**9** was partial intercalation and **8** had stronger insertion capability [18].

3.3. Protein binding studies

Bovine serum albumin (BSA) was used as model protein to investigate the interactions of **8** and **9** with protein, due to its structural homology with human serum albumin (HSA) [1]. Fluorescence quenching experiment was taken to measure the effects of **8** and **9** on the intrinsic fluorescence of BSA. When BSA is excited at 280 nm, its fluorescence is mainly ascribed to the 212-positioned tryptophan residue (Trp) which is highly sensitive to the surrounding environment [19]. It is observed that the fluorescence intensity of BSA decreased with the addition of increasing amounts of **8** and **9**, and the maximum wavelength of fluorescence intensity at 348 nm was reduced by 40.64% (**8**) and 41.49% (**9**), respectively, with no change of peak shape and position (Fig. 6). The occurrence of fluorescence quenching suggests that the interaction of **8** and **9** with BSA had pronounced effects on the surrounding environment of Trp.

The fluorescence quenching of BSA caused by **8** and **9** can be described with the following Stern-Volmer equation [20].

$$F_0/F = 1 + K_{sv}[Q] = 1 + K_q\tau_0[Q] \quad (2)$$

F_0 and F represent the emission intensities of BSA in the absence and presence of the quencher (**8**/**9**), respectively; K_{SV} represents the Stern-Volmer quenching constant [20], represents the concentration of the

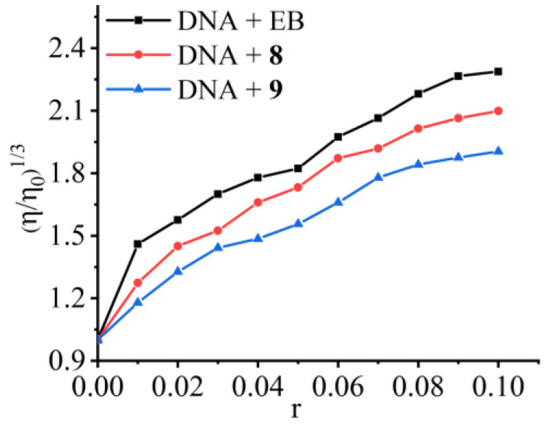

Fig. 5. The relative viscosity of CT DNA in the presence of EB, **8** and **9** at 298 K and pH 7.2, [DNA] = 1.0×10^{-4} M, r = [EB/**8**/**9**]/[DNA] = 0, 0.01, 0.02, 0.03, 0.04, 0.05, 0.06, 0.07, 0.08, 0.09, 0.1, respectively.

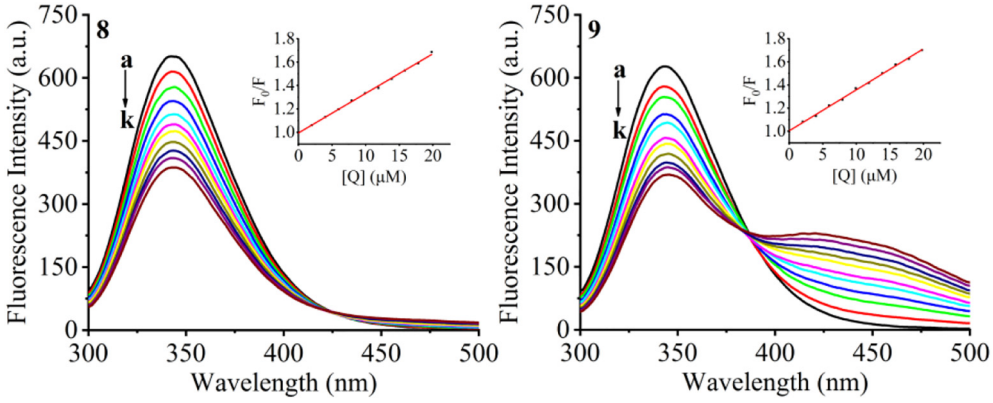

Fig. 6. Effects of **8** and **9** on the fluorescence spectra of BSA at 298 K and pH 7.0, [BSA] = 3.0×10^{-6} M, [Quencher]/[BSA] = 0, 0.66, 1.33, 1.98, 2.64, 3.3, 3.96, 4.62, 5.28, 5.94, 6.60, respectively. Insets: plot of F_0/F versus [Quencher].

quencher, K_q represents the biomolecular quenching rate constant, and τ_0 is the protein fluorescence lifetime in the absence of the quencher (10^{-8} s for BSA) [20]. The quenching of BSA fluorescence fit well with the linear Stern-Volmer equation (Fig. 6, insets), suggesting there was only a single type of quenching mechanism during the interaction process [20]. The K_{SV} values for **8** and **9** were 3.38×10^4 M^{-1} and 3.54×10^4 M^{-1}, respectively. The obtained K_q for **8** (3.38×10^{12} M^{-1} S^{-1}) and **9** (3.54×10^{12} M^{-1} S^{-1}) were 100-fold higher than the maximum scattering collision quenching constant (2×10^{10} M^{-1} S^{-1}), proving the quenching process was dominant by static quenching one [20]. The above results propose that **8** and **9** could bind efficiently with BSA.

Synchronous fluorescence technique is generally used to detect the changes of protein conformation due to its selectivity and sensitivity. When BSA binds with small molecules, there will be some changes in the microenvironment and conformation around the vicinity of tyrosine (Tyr) and tryptophan (Trp) [1]. In synchronous fluorescence spectra, the wavelength interval ($\Delta\lambda$) between emission and excitation can reflect the characteristics of chromophores (Tyr or Trp). When $\Delta\lambda$ are set at 15 nm or 60 nm, the corresponding chromophore Tyr or Trp will be responsible for the emission of fluorescence, respectively [1]. With the increase of the concentrations of **8** and **9** added to BSA, the fluorescence intensity for both the Tyr and the Trp were quenched to some extent, along with 2 nm (**8**) and 3 nm (**9**) red shift for Tyr and no shift for Trp, respectively (Fig. 7). This result reveals that the interactions between the compounds with BSA affected the microenvironment of Tyr and Trp, i.e., the hydrophobicity of BSA was decreased and the polarity of BSA was increased [21].

Circular dichroism was used to further detect the effects of **8** and **9** on the secondary structure of BSA, because synchronous fluorescence assay showed that the microenvironment of Tyr and Trp have been changed upon the interactions with them. It can be observed that the addition of **8** and **9** into BSA solution has greatly changed the characteristic CD signals of BSA at 209 nm and 220 nm, including the intensity

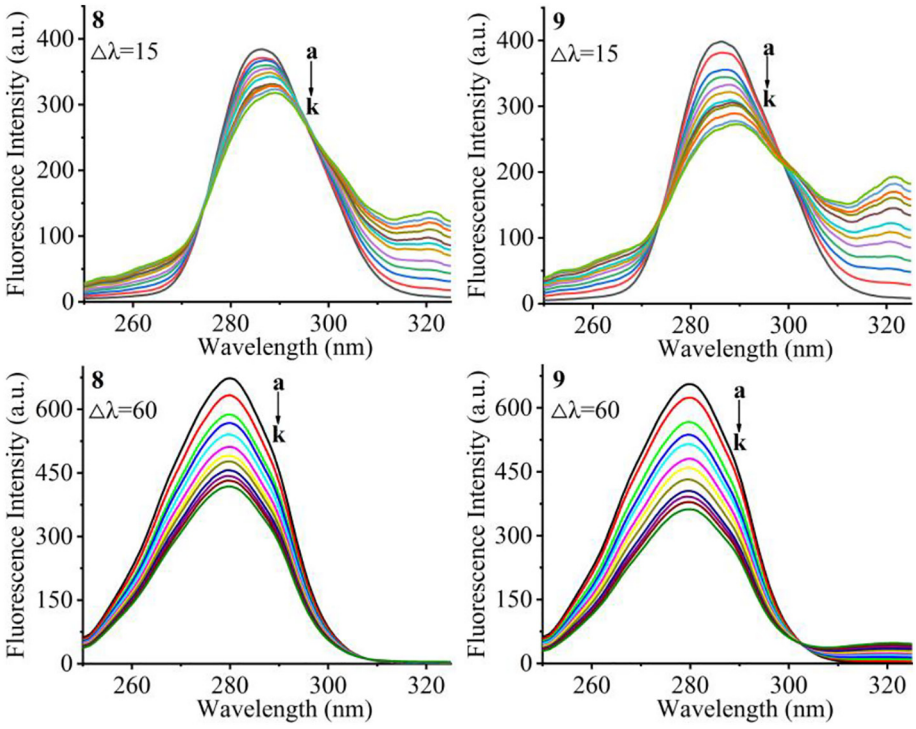

Fig. 7. Synchronous fluorescence spectra ($\Delta\lambda = 15$ nm and $\Delta\lambda = 60$ nm) of BSA in the absence and presence of various **8**/**9** concentrations, at 298 K and pH 7.0, [BSA] = 3.0×10^{-6} M, [**8**/**9**]/[BSA] = 0, 0.66, 1.33, 1.98, 2.64, 3.3, 3.96, 4.62, 5.28, 5.94, 6.60, respectively.

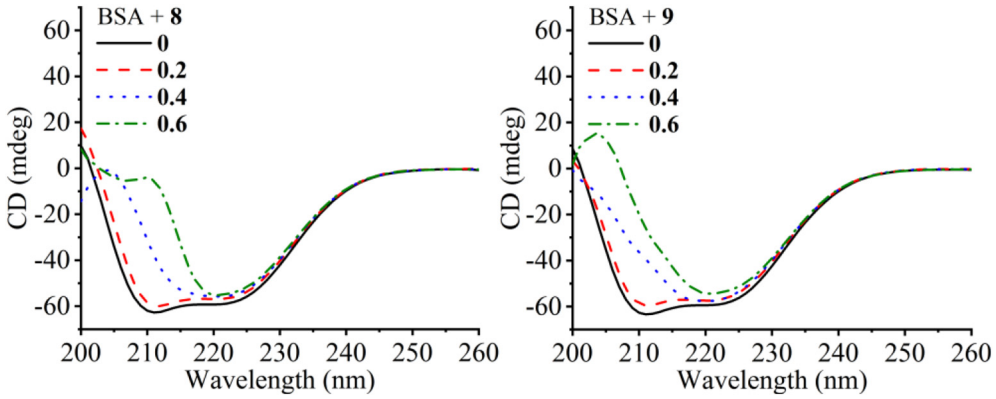

Fig. 8. Effects of **8** and **9** on the CD spectra of BSA at 298 K and pH 7.0, [BSA] = 5.0×10^{-7} M, [**8**/**9**]/[BSA] = 0, 0.2, 0.4 and 0.6, respectively.

Table 2
IC_{50} (μM ± SD) values of **3**, **8**, **9**, cisplatin and oxaliplatin toward the selected cancer cell lines. Cells were treated for 48 h.

Cell lines	Cisplatin	Oxaliplatin	**3**[a]	**8**[b]	**9**
HepG2	7.63 ± 1.60	>20	>20	>20	>20
MCF-7	6.30 ± 0.42	7.59 ± 1.50	>20	8.04 ± 1.64	13.35 ± 0.45
HeLa	13.05 ± 3.04	>20	>20	15.09 ± 0.62	>20
A431	10.50 ± 0.88	15.75 ± 3.59	>20	8.75 ± 0.49	>20
A549	5.34 ± 1.00	7.09 ± 0.16	11.89 ± 0.66	>20	>20

[a] The data were from ref. [4].
[b] The data were from ref. [1].

and type of the bands, and this tendency was related to the concentrations of the compounds, i.e., the higher the concentration, the more obvious the change (Fig. 8). Such result means that the conformational changes of BSA created by the interaction with **8** and **9** have facilitated BSA to lose some α-helix characteristics [1].

3.4. In vitro cytotoxicity

The in vitro cytotoxicities of **3**, **8** and **9** toward human cancer cells including liver hepatocellular carcinoma HepG2, breast carcinoma MCF-7, cervical carcinoma HeLa, epidermoid carcinoma A431 and lung carcinoma A549 were evaluated by MTT assay, with clinical used drugs cisplatin and oxaliplatin as positive controls, and the half maximal inhibitory concentration IC_{50} values listed in Table 2. Their sensitivity to the selected cells were varied, **8** was sensitive to MCF-7, HeLa and A431 cells, **9** was sensitive to MCF-7 cell, while **3** was sensitive to A549 cell. In MCF-7 cell line assay, the cytotoxicities of cisplatin (IC_{50} = 6.30 ± 0.42 μM), oxaliplatin (IC_{50} = 7.59 ± 1.50 μM) and **8** (IC_{50} = 8.04 ± 1.64 μM) were similar and better than that of **9** (IC_{50} = 13.35 ± 0.45 μM), and **8** and **9** were more cytotoxic than **3**. In A431 cell line assay, the cytotoxicity of **8** (IC_{50} = 8.75 ± 0.49 μM) was better than that of cisplatin (IC_{50} = 10.50 ± 0.88 μM) and oxaliplatin (IC_{50} = 15.75 ± 3.59 μM). In HeLa cell line assay, the cytotoxicity followed the order of cisplatin > **8** > oxaliplatin. Based on the above results, we can draw the conclusion that the introduction of amide and pyridine significantly improved the cytotoxicity of **3**, but more than one amide and pyridine units in the target compound **9** reduced the cytotoxicity compared with **8**. The data in Table 2 indicate that **8** and **9** do not have a broad spectrum of cytotoxicity, which may be related to the nature of cells. The anticancer activity of **8** is worth further and deeper study.

4. Conclusions

In summary, two DHA derivatives DTPC and DDTPC bearing pyridine and amide moieties were designed and synthesized in order to find more effective anticancer candidate based on natural product rosin. They could bind with CT DNA through partial intercalation and the binding ability of DTPC was stronger. They could also bind with BSA and make BSA lose some α-helix characteristics. The BSA affinity of DDTPC was higher. MTT assay show that they possessed selective cytotoxicity toward human cancer cells, and DTPC was better than DDTPC in terms of inhibiting the proliferation of tumor cells. DTPC displayed better cytotoxic activity than clinical used cisplatin and oxaliplatin toward A431 cell line. Their cytotoxicity followed the order of their DNA binding ability.

CRediT authorship contribution statement

Lin-Ying Li: Writing - original draft. **Bao-Li Fei:** Conceptualization, Methodology, Funding acquisition. **Pingping Wang:** Investigation, Data curation. **Ling-Yan Kong:** Writing - review & editing. **Jian-Ying Long:** Data curation.

Declaration of competing interest

There is no conflict of interest for this paper.

Acknowledgments

The authors acknowledge the financial support from State Key Laboratory for Chemistry and Molecular Engineering of Medicinal Resources (Guangxi Normal University) (CMEMR2018-B13), the Priority Academic Program Development of Jiangsu Higher Education Institutions and Major Projects of Natural Science Research of Jiangsu Higher Education Institutions of China (18KJA150006).

Appendix A. Supplementary data

Supplementary data to this article can be found online at https://doi.org/10.1016/j.saa.2020.118944.

References

[1] B.L. Fei, S.Y. Tu, Z.Z. Wei, P.P. Wang, J.Y. Long, C.H. Qiao, Z.F. Chen, Biological evaluation of optically pure chiral binuclear copper(II) complexes based on a rosin derivative as highly potential anticancer agents, Dalton Trans. 48 (2019) 15646–15656.

[2] J.J. Chen, B.L. Song, X.M. Pei, Z.G. Cui, D.H. Xie, Rheological behavior of environmentally friendly viscoelastic solutions formed by a rosin-based anionic surfactant, J. Agric. Food Chem. 67 (2019) 2004–2011.

[3] P. Tao, C.Y. Wu, J. Hao, Y.Q. Gao, X.H. He, J. Li, S.B. Shang, Z.Q. Song, J. Song, Antifungal application of rosin derivatives from renewable pine resin in crop protection, J. Agric. Food Chem. 68 (2020) 4144–4154.

[4] B.L. Fei, S.Y. Tu, Z.Z. Wei, P.P. Wang, J.Y. Long, C.H. Qiao, Z.F. Chen, Optically pure chiral copper(II) complexes of rosin derivative as attractive anticancer agents with potential anti-metastatic and anti-angiogenic activities, Eur. J. Med. Chem. 176 (2019) 175–186.

[5] M. Marloye, G. Berger, M. Gelbcke, F. Dufrasne, A survey of the mechanisms of action of anticancer transition metal complexes, Future Med. Chem. 8 (2016) 2263–2286.

[6] J. Akhtar, A.A. Khan, Z. Ali, R. Haider, M.S. Yar, Structure-activity relationship (SAR) study and design strategies of nitrogen-containing heterocyclic moieties for their anticancer activities, Eur. J. Med. Chem. 125 (2017) 143–189.

[7] S.K. Chaturvedi, E. Ahmad, J.M. Khan, P. Alam, M. Ishtikhar, R.H. Khan, Elucidating the interaction of lLimonene with bovine serum albumin: a multi-technique approach, Mol. BioSyst. 11 (2015) 307–316.

[8] N. Sjakste, N. Djelic, M. Dzintare, L. Zivkovic, DNA-binding and DNA-protecting activities of small natural organic molecules and food extracts, Chem. Biol. Interact. 323 (2020) 109030.

[9] Y.W. Liu, H.J. Cheng, B.F. Ruan, Q. Hu, Synthesis, characterization and antitumor activity of (E)-2-methyl-3-ferrocenyl-N-acrylamide derivatives, J. Organomet. Chem. 887 (2019) 71–79.

[10] B.L. Fei, W. Li, W.S. Xu, J.Y. Long, Q.B. Liu, W.Y. Sun, C.E. Anson, A.K. Powell, Synthesis, crystal structure, DNA binding, antibacterial, and cytotoxic activities of two chiral cCopper(II) complexes, Eur. J. Inorg. Chem. 34 (2013) 5919–5927.

[11] S. Vudhgiri, D. Koude, D.K. Veeragoni, S. Misra, R.B.N. Prasad, R.C.R. Jala, Synthesis and biological evaluation of 5-fatty-acylamido-1,3, 4-thiadiazole-2-thioglycosides, Bioorg. Med. Chem. Lett. 27 (2017) 3370–3373.

[12] I.H. Krakoff, M.E. Balis, Studies of the uricogenic effect of 2-substituted thiadiazoles in man, J. Clin. Invest. 38 (1959) 907–915.

[13] M. Keenan, M.J. Abbott, P.W. Alexander, T. Armstrong, W.M. Best, B. Berven, A. Botero, J.H. Chaplin, S.A. Charman, E. Chatelain, T.W. von Geldern, M. Kerfoot, A. Khong, T. Nguyen, J.D. McManus, J. Morizzi, E. Ryan, I. Scandale, R.A. Thompson, S.Z. Wang, K.L. White, Analogues of fenarimol are potent inhibitors of trypanosoma cruzi and are efficacious in a murine model of chagas disease, J. Med. Chem. 55 (2012) 4189–4204.

[14] J.M. Aizpurua, C. Palomo, R.M. Fratila, P. Ferrón, A. Benito, E. Gomez-Bengoa, J. Miranda, J.I. Santos, Mechanistic insights on the magnesium(II) ion-activated reduction of methyl benzoylformate with chelated NADH peptide beta-lactam models, J. Org. Chem. 74 (2009) 6691–6702.

[15] B.L. Fei, W.S. Xu, H.W. Tao, W. Li, Y. Zhang, J.Y. Long, Q.B. Liu, B. Xia, W.Y. Sun, Effects of copper ions on DNA binding and cytotoxic activity of a chiral salicylidene Schiff base, J. Photochem. Photobiol. B 132 (2014) 36–44.

[16] M. Dehkhodaei, M. Sahihi, H.A. Rudbari, F. Momenbeik, DNA and HSA interaction of vanadium (IV), copper (II), and zinc (II) complexes derived from an asymmetric bidentate Schiff-base ligand: multi spectroscopic, viscosity measurements, molecular docking, and ONIOM studies, J. Biol. Inorg. Chem. 23 (2018) 181–192.

[17] A.K.F. Martensson, M. Abrahamsson, E.M. Tuite, P. Lincoln, Diastereomeric crowding effects in the competitive DNA intercalation of Ru(phenanthroline)$_2$dipyridophenazine^{2+} enantiomers, Inorg. Chem. 58 (2019) 9452–9459.

[18] C. Gan, X. Huang, J. Zhan, X. Liu, Y. Huang, J. Cui, Study on the interactions between B-norcholesteryl benzimidazole compounds with ct-DNA, Spectrochim. Acta A 227 (2020) 117525.

[19] A.G. Ribeiro, S.M.V. de Almeida, J.F. de Oliveira, T.R.C.D. Souza, K.L. dos Santos, A.P.D. Albuquerque, M.C.D.L. Nogueira, L.B. de Carvalho, R.O. de Moura, A.C. de Silva, V.R.A. Pereira, M.C.A.B. de Castro, M.D.A. de Lima, Novel 4-quinoline-thiosemicarbazone derivatives: synthesis, antiproliferative activity, in vitro and in silico biomacromolecule interaction studies and topoisomerase inhibition, Eur. J. Med. Chem. 182 (2019) 111592.

[20] T. Topala, A. Pascual-Alvarez, M.A. Moldes-Tolosa, A. Bodoki, A. Castineiras, J. Torres, C. del Pozo, J. Borras, G. Alzuet-Pina, New sulfonamide complexes with essential metal ions [Cu(II), Co(II), Ni(II) and Zn(II)]. Effect of the geometry and the metal ion on DNA binding and nuclease activity. BSA protein interaction, J. Inorg. Biochem. 202 (2020), 110823, .

[21] M.M. Alam, F.A. Qais, I. Ahmad, P. Alam, R.H. Khan, I. Naseem, Multi-spectroscopic and molecular modelling approach to investigate the interaction of riboflavin with human serum albumin, J. Biomol. Struct. Dyn. 36 (2018) 795–809.